PERGAMON

International Journal of Solids and Structures 38 (2001) 7587–7606

INTERNATIONAL JOURNAL OF SOLIDS and STRUCTURES

www.elsevier.com/locate/ijsolstr

Interfacial thermal stress analysis of an elliptic inclusion with a compliant interphase layer in plane elasticity

H. Shen [1], P. Schiavone *, C.Q. Ru, A. Mioduchowski

Department of Mechanical Engineering, University of Alberta, 4-9, Mechanical Engineering Building, Edmonton, Alberta, Canada T6G 2G8

Received 15 March 2000

Abstract

Stresses induced by thermal mismatch are known to be a major cause of failure in a wide variety of composite materials and devices ranging from metal–ceramic composites to passivated interconnect lines in integrated circuits. One of the most effective procedures used to reduce these thermal stresses is the addition of a compliant intermediate or interphase layer between the different material components.

This paper is concerned with the interfacial thermal stress analysis of an elliptic inclusion embedded within an infinite matrix with uniform change in temperature. A compliant interphase layer is assumed to occupy the region between the inclusion and the matrix. This interphase layer is modeled as a spring layer with vanishing thickness (henceforth referred to as the *interface* between the inclusion and the matrix). Its behavior is based on the assumption that tractions are continuous but displacements are discontinuous across the interface.

Complex variable techniques are used to obtain infinite series representations of the thermal stresses which, when evaluated numerically, demonstrate how the peak interfacial thermal stresses vary with the aspect ratio of the inclusion and the parameter h describing the interface. In addition, and perhaps most significantly, for different aspect ratios of the elliptic inclusion, we identify a specific value (h^*) of the interface parameter h which corresponds to the maximum peak thermal stress along the inclusion–matrix interface. Similarly, for different aspect ratios, we identify a specific value of h (also referred to as h^* in the paper) which corresponds to the peak maximum thermal strain energy density along the interface (J. Appl. Mech. 57 (1990) 956–963). In each case, we plot the relationship between the new parameter h^* and the aspect ratio of the ellipse. This gives significant and valuable information regarding the failure of the interface using two established failure criteria.

Keywords: Voids and inclusions; Stress concentrations; Elastic material; Fibre-reinforced composite material; Imperfect interface

* Corresponding author. Tel.: +1-780-492-3598; fax: +1-780-492-2200.
E-mail address: p.schiavone@ualberta.ca (P. Schiavone).
[1] Graduate student.

0020-7683/01/$ - see front matter
PII: S0020-7683(01)00033-6

1. Introduction

Mechanical failure resulting from residual stresses induced by thermal mismatch in composite materials and electromechanical devices has received considerable attention recently (see, e.g., Wikström et al., 1999; Gouldstone et al., 1998; Ru, 1998a; Shen, 1998; Dao et al., 1997; Gleixner et al., 1997; Wu et al., 1996; Lee and Erdogan, 1995; Yeo et al., 1995; Williamson et al., 1993). Most of the existing studies have focused on multilayered material systems. However, many practical problems require a systematic study of the effects of interphase layers on thermal mismatch induced stresses in inclusion/matrix systems. For example, the failure of interconnect lines due to thermal stress-induced voiding has become a major issue in the design of reliable integrated circuits. In this case, the line is subjected to large tensile stresses upon cooling from high passivation deposition temperatures. For example, Niwa et al. (1990) and Korhonen et al. (1991) have modeled the passivated line as an elongated ellipsoid surrounded by an infinite homogeneous matrix. One of the most effective procedures for the reduction of thermal stresses concerns the addition of an intermediate layer, with appropriate geometry and thermomechanical properties, between different material components where elevated thermal stresses occur. This procedure has been widely used in many practical problems where the thermal mismatch-induced stresses are of vital importance to mechanical integrity, such as thermal barrier coatings (see, e.g., Lee and Erdogan, 1995), electromechanical devices (see, e.g., Wu et al., 1996), and metal–ceramic composites (see, e.g., Williamson et al., 1993). In doing so, the problem is reduced to one of the analysis of thermal stresses within an elliptic inclusion surrounded by an interphase layer. Unfortunately, in contrast to the well-known uniform stress state within a single elliptic inclusion perfectly bonded to the surrounding (infinite) matrix, the stress field within an elliptic inclusion surrounded by an interphase layer is extremely complicated and intrinsically non-uniform (see, e.g., Shen et al., 2000a,b). In particular, to isolate the role of thermal mismatch, Niwa et al. (1990, 1992) have neglected the elastic mismatch between the line and the surrounding materials. Very recently, Ru (1998a) studied the thermal stresses within a three-phase elliptical inclusion with the similar simplification. Especially, Ru (1998a) also assumed the interphase layer is bounded by two confocal ellipses. However, the more realistic case is the "equal thickness" interphase layer, which corresponds to the present interface model (h = constant). Recently, for anti-plane shear deformations, Ru et al. (1999) proved that the residual/thermal stress can be reduced to a fraction of its original value when a compliant interphase layer is inserted between the elliptic inclusion and its surrounding matrix. Of greater theoretical and practical interest, however, is the corresponding plane problem. Namely, the effect of a compliant interphase layer on the thermal stresses induced by the plane-strain deformations of an elliptic inclusion.

In many cases, the compliant layer between the inclusion and the surrounding material (matrix) may be considered to be a very thin interphase layer, referred to in the literature as an *imperfect interface*. Problems involving an elastic inclusion with imperfect interface have received a considerable amount of attention in the literature (see, e.g., Ru and Schiavone, 1997; Hashin, 1990, 1991a,b; Jasiuk and Tong, 1989; Gao, 1995; Tsuchida et al., 1986). Interest in these problems is motivated by the study of interface damage in composites (e.g., debonding, sliding and/or cracking across an interface) and its subsequent effect on material properties. One of the more widely used models of an imperfect interface (see, e.g., Achenbach and Zhu, 1989, 1990; Hashin, 1990, 1991a,b; Gao, 1995) is based on the assumption that tractions are continuous but displacements are discontinuous across the interface. More precisely, jumps in the displacement components are assumed to be proportional, in terms of 'spring-factor-type' interface parameters, to their respective interface traction components. According to Hashin (1991b), the imperfect interface model is appropriate for a thin compliant interphase layer with very small shear modulus (compared to inclusion and matrix). When the compliant interphase layer is of "equal thickness", the corresponding imperfect interface parameters are uniform along the entire length of the material interface and the interface is referred to as *homogeneously imperfect*. Using this model, Hashin (1991b) examined the case of a spherical inclusion imperfectly bonded to a three-dimensional matrix. In contrast to the case of perfect bonding,

Hashin found that, under a remote uniform stress field, the state of stress inside the inclusion is no longer uniform. The analogous result in plane elasticity has been established by Gao (1995) for a circular inclusion and Qu (1993) for an elliptic inclusion with the so-called "weakened interface". However, to the authors' knowledge, the solution of the problem associated with plane deformations of an elliptic inclusion with a homogeneously imperfect interface (or compliant interphase layer) subjected to a uniform change in temperature has not been recorded in the literature.

In this paper, we use the homogeneously imperfect interface model mentioned above to study the effect of a compliant interphase layer on thermal stresses in an elliptic elastic inclusion embedded within an infinite matrix under a uniform change in temperature. Both elastic mismatch and thermal mismatch will be considered. It is well known that the interphase layer is often the site of nucleation of damage and voids or cracks. In some instances, interfacial separation leads directly to catastrophic failure, while in other circumstances failure results from void nucleation as a result of a sequence of inclusion decohesion events. Consequently, it is of practical interest to examine the interfacial stresses in the presence of a compliant interphase layer. Using complex variable techniques we obtain infinite series representations of the corresponding stresses which, when evaluated numerically, demonstrate how the peak thermal interfacial stress varies with the parameter h describing the imperfect interface (the interphase layer). Perhaps most significant is the fact that our results demonstrate that the peak thermal stress along the interface is a non-monotonic function of h. This allows us to identify a specific value h^* of the interface parameter which corresponds to the maximum peak thermal stress along the inclusion–matrix interface. We also identify another value (also referred to as h^*) of h which corresponds to the maximum peak thermal interfacial strain energy density as defined by Achenbach and Zhu (1990). In each case, we plot the relationship between this new parameter (h^*) and the aspect ratio of the ellipse. This gives significant and valuable information regarding the failure of the interface using two different yet well-established failure criteria.

2. Problem formulation

Consider a domain in $\mathbb{R}^2$, infinite in extent, containing a single internal elastic inclusion with elastic properties different from those of the surrounding matrix. The linearly elastic materials occupying the matrix and the inclusion are assumed to be homogeneous and isotropic with associated shear moduli μ_1 and μ_2, respectively. We represent the matrix by the domain S_1 and assume that the inclusion occupies an elliptic region S_2 with center at the origin of the coordinate system. The ellipse Γ will denote the inclusion–matrix interface. In what follows, the subscripts 1 and 2 will refer to the regions S_1 and S_2, respectively and (x, y) will denote a generic point in $\mathbb{R}^2$ referred to a Cartesian coordinate system.

It is well known that for plane deformations, the displacement components (u_x, u_y), stress (or traction) components $(\sigma_{xx}, \sigma_{yy}, \sigma_{xy})$ and the components of the resultant force (F_x, F_y) are given in terms of two analytic functions $\phi(z)$ and $\psi(z)$ by (Muskhelishvili, 1963):

$$2\mu(u_x + \mathrm{i}u_y) = \kappa\phi(z) - z\overline{\phi'(z)} - \overline{\psi(z)}, \tag{2.1}$$

$$\sigma_{xx} + \sigma_{yy} = 2\left[\phi'(z) + \overline{\phi'(z)}\right], \tag{2.2}$$

$$\sigma_{yy} - \sigma_{xx} + 2\mathrm{i}\sigma_{xy} = 2\left[\bar{z}\phi''(z) + \psi'(z)\right], \tag{2.3}$$

$$F_x + \mathrm{i}F_y = -\mathrm{i}\left[\phi(z) + z\overline{\phi'(z)} + \overline{\psi(z)}\right]_p^q. \tag{2.4}$$

Here, $z = x + iy$ is the complex coordinate, v is Poisson's ratio, $\kappa = 3 - 4v$ for plane strain and $(3 - v)/(1 + v)$ for plane stress, and $[\ ]_p^q$ represents the change in the corresponding function in moving from point p to point q along any arc pq.

Across the interface Γ, the boundary displacements and tractions are written in normal-tangential $((n,t)-)$ coordinates as:

$$2\mu(u_n + iu_t) = \left[\kappa\phi(z) - z\overline{\phi'(z)} - \overline{\psi(z)}\right]e^{-i\alpha(z)}, \tag{2.5}$$

$$\sigma_{nn} - i\sigma_{nt} = \phi'(z) + \overline{\phi'(z)} - [\bar{z}\phi''(z) + \psi'(z)]e^{2i\alpha(z)}, \tag{2.6}$$

where n is the outward unit normal at $z \in \Gamma$ which also is represented, in complex form, by $e^{i\alpha(z)}$ (where α defines the angle between the normal direction n and the positive x-axis). Assume that the elliptic inclusion is bonded to the matrix by a homogeneously imperfect interface as described in Section 1. The interface conditions are then given by

$$[[\sigma_{nn} - i\sigma_{nt}]] = 0, \qquad \sigma_{nn} = h_1[[u_n]] - h_1u_n^0, \qquad \sigma_{nt} = h_2[[u_t]] - h_2u_t^0 \quad \text{on } \Gamma. \tag{2.7}$$

Here h_1 and h_2 are two non-negative interface parameters (basically the 'spring-type constants' of the interface model having dimension of stress divided by length) and $[[*]] = (*)_1 - (*)_2$ denotes the jump across Γ. u_n^0 and u_t^0 are the displacements induced by the uniform (stress-free) eigenstrains $(\varepsilon_{xx}^0, \varepsilon_{yy}^0, \varepsilon_{xy}^0)$. The classical case of perfect bonding is obtained from our model in the limiting case when $h_1 = h_2 = \infty$. Similarly, the case of pure sliding can be obtained by setting $h_2 = 0$ and $h_1 = \infty$ while the completely debonded interface can be described by setting $h_1 = h_2 = 0$. Any remaining finite positive values of h_1 and h_2 represent the imperfectly bonded interface considered in this paper.

If we consider only residual stresses resulting from eigenstrains, the stresses at infinity must be zero. Thus, the asymptotic conditions at infinity are given by

$$\phi_1(z) \cong 0(1), \qquad \psi_1(z) \cong 0(1), \quad |z| \to \infty, \tag{2.8}$$

From Eq. (2.7) we can now write

$$\sigma_{nn} - i\sigma_{nt} = \frac{(h_1 - h_2)}{2}[[(u_n + iu_t)]] + \frac{(h_1 + h_2)}{2}[[(u_n - iu_t)]] - [h_1u_n^0 - ih_2u_t^0], \tag{2.9}$$

where, from Eq. (2.5), we have

$$\begin{aligned} 2[[u_n + iu_t]] &= \frac{e^{-i\alpha(z)}}{\mu_1}\left[\kappa_1\phi_1(z) - z\overline{\phi_1'(z)} - \overline{\psi_1(z)}\right] - \frac{e^{-i\alpha(z)}}{\mu_2}\left[\kappa_2\phi_2(z) - z\overline{\phi_2'(z)} - \overline{\psi_2(z)}\right], \\ 2[[u_n - iu_t]] &= \frac{e^{i\alpha(z)}}{\mu_1}\left[\kappa_1\overline{\phi_1(z)} - \bar{z}\phi_1'(z) - \psi_1(z)\right] - \frac{e^{i\alpha(z)}}{\mu_2}\left[\kappa_2\overline{\phi_2(z)} - \bar{z}\phi_2'(z) - \psi_2(z)\right], \quad \text{on } \Gamma \end{aligned} \tag{2.10}$$

and

$$-[h_1u_n^0 - ih_2u_t^0] = -\frac{h_1 - h_2}{2}[\varepsilon_1 z + (\varepsilon_2 + i\varepsilon_3)\bar{z}]e^{-i\alpha(z)} - \frac{h_1 + h_2}{2}[\varepsilon_1\bar{z} + (\varepsilon_2 - i\varepsilon_3)z]e^{i\alpha(z)}, \quad \text{on } \Gamma. \tag{2.11}$$

Here,

$$\varepsilon_1 \equiv \frac{\varepsilon_{xx}^0 + \varepsilon_{yy}^0}{2}, \qquad \varepsilon_2 \equiv \frac{\varepsilon_{xx}^0 - \varepsilon_{yy}^0}{2}, \qquad \varepsilon_3 \equiv \varepsilon_{xy}^0.$$

The geometry of the problem is simplified by mapping the ellipse into the unit circle using the following mapping function (Fig. 1) (Muskhelishvili, 1963):

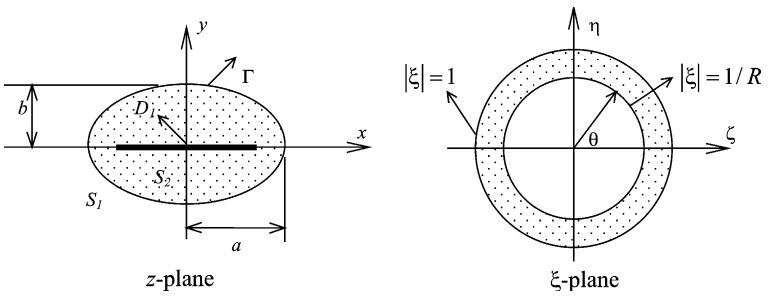

Fig. 1. Conformal mapping from z-plane to ξ-plane.

$$z = m(\xi) = \frac{l}{2}\left(R\xi + \frac{1}{R\xi}\right), \qquad R\xi = \frac{z}{l}\left\{1 + \left[1 - \left(\frac{l}{z}\right)^2\right]^{1/2}\right\}, \qquad \xi = \zeta + \mathrm{i}\eta = r\mathrm{e}^{\mathrm{i}\theta}. \tag{2.12}$$

Here,

$$R = \sqrt{\frac{a+b}{a-b}} > 1 \quad \text{and} \quad l = \sqrt{a^2 - b^2}. \tag{2.13}$$

We imagine the enclosed region S_2 to be cut along the segment $D_1 = \{(x,0): -l \leqslant x \leqslant l\}$ connecting the foci. This cut may be thought of as an ellipse, which is confocal with Γ but whose minor axis is zero. Hence the cut region in S_2 may be thought of as the limiting case of a region between two confocal ellipses. If in the cut ellipse (S_2),

$$\phi_2(z) = \phi_2(\bar{z}), \qquad \psi_2(z) = \psi_2(\bar{z}), \quad z \in D_1, \tag{2.14}$$

the functions ϕ_2 and ψ_2 will take only one and the same value when the point z approaches the segment D_1 from either side. Consequently, the conditions (2.14) ensure that ϕ_2 and ψ_2 are analytic functions throughout the domain S_2.

For convenience, we write $\phi(\xi) = \phi(m(\xi))$ and $\psi(\xi) = \psi(m(\xi))$ so that in the mapped ξ-plane, the displacements, stresses and resultant forces take the form

$$2\mu(u_x + \mathrm{i}u_y) = \kappa\phi(\xi) - m(\xi)\overline{\Phi(\xi)} - \overline{\psi(\xi)}, \tag{2.15}$$

$$\sigma_{xx} + \sigma_{yy} = 2\left[\Phi(\xi) + \overline{\Phi(\xi)}\right], \tag{2.16}$$

$$\sigma_{yy} - \sigma_{xx} + 2\mathrm{i}\sigma_{xy} = 2\left[\Phi'(\xi)\frac{\overline{m(\xi)}}{m'(\xi)} + \Psi(\xi)\right], \tag{2.17}$$

$$F_x + \mathrm{i}F_y = -\mathrm{i}\left[\phi(\xi) + m(\xi)\overline{\Phi(\xi)} + \overline{\psi(\xi)}\right]_p^q, \tag{2.18}$$

respectively. Here, the prime denotes differentiation with respect to ξ, $\Phi(\xi) = \phi'(\xi)/m'(\xi)$ and $\Psi(\xi) = \psi'(\xi)/m'(\xi)$. Similarly, the condition (2.14) becomes:

$$\phi_2(\xi) = \phi_2(\bar{\xi}), \qquad \psi_2(\xi) = \psi_2(\bar{\xi}), \quad \forall \xi : |\xi| = 1/R. \tag{2.19}$$

The condition that tractions be continuous across the interface may be integrated to become a resultant continuity condition of the form:

$$\left(F_x + \mathrm{i}F_y\right)_1 = \left(F_x + \mathrm{i}F_y\right)_2. \tag{2.20}$$

For convenience, we introduce an auxiliary stress function $\Omega(\xi)$ (Stagni, 1991) such that

$$\Omega(\xi) = \frac{\overline{m(1/\overline{\xi})}}{m'(\xi)}\phi'(\xi) + \psi(\xi). \tag{2.21}$$

Thus, using Eqs. (2.18), (2.20) and (2.21), continuity of tractions across the interface may be expressed in the form:

$$\phi_1(\xi) + \overline{\Omega_1(\xi)} = \phi_2(\xi) + \overline{\Omega_2(\xi)}, \quad |\xi| = 1. \tag{2.22}$$

The complex potentials $\phi_\alpha(\xi)$ and $\Omega_\alpha(\xi)$ are now expanded into their respective Laurent series in the matrix and in the inclusion as follows:

$$\phi_1(\xi) = \sum_{n=0}^{\infty} A_n \xi^{-(n+1)}, \qquad \Omega_1(\xi) = \sum_{n=0}^{\infty} C_n \xi^{-(n+1)}, \tag{2.23}$$

$$\phi_2(\xi) = \sum_{n=0}^{\infty} (S_n \xi^{n+1} + T_n \xi^{-(n+1)}), \qquad \Omega_2(\xi) = \sum_{n=0}^{\infty} (D_n \xi^{n+1} + E_n \xi^{-(n+1)}). \tag{2.24}$$

Note that the constant terms have been omitted since they have no effect on the stress distribution. Furthermore, Eq. (2.19) combined with Eqs. (2.23) and (2.24) yields the following relation (Gong and Meguid, 1993; Stagni, 1991):

$$T_n = \frac{S_n}{R^{2n+2}}, \qquad E_n = \frac{D_n}{R^{2n+2}} + \frac{(n+1)S_n}{R^{2n+4}}(R^4 - 1), \quad (n = 0, 1, 2, 3 \ldots). \tag{2.25}$$

Consequently, Eq. (2.25) allows us to express the coefficients T_n, E_n in terms of the coefficients D_n, S_n. The traction continuity condition (2.22) now becomes:

$$\sum_{n=0}^{\infty} A_n \xi^{-(n+1)} - \sum_{n=0}^{\infty} \overline{D}_n \overline{\xi}^{n+1} + \sum_{n=0}^{\infty} (\overline{C}_n - \overline{E}_n)\overline{\xi}^{-(n+1)} = \sum_{n=0}^{\infty} (S_n \xi^{n+1} + T_n \xi^{-(n+1)}). \tag{2.26}$$

Noting that $\xi = \mathrm{e}^{\mathrm{i}\theta}$ on the interface, comparing coefficients, we obtain

$$\overline{C}_n = \overline{E}_n + S_n, \qquad C_n = E_n + \overline{S}_n, \quad (n = 0, 1, 2, 3 \ldots), \tag{2.27}$$

$$\overline{A}_n = \overline{T}_n + D_n, \qquad A_n = T_n + \overline{D}_n, \quad (n = 0, 1, 2, 3 \ldots). \tag{2.28}$$

Thus the coefficients A_n, C_n can be expressed in terms of the coefficients D_n, S_n. The only unknown coefficients are therefore D_n and S_n. These can obtained from the interface condition (2.9) as follows.

In the mapped ξ-plane, noting the following relations from England (1971),

$$\mathrm{e}^{\mathrm{i}2\alpha(z)} = \frac{\xi^2}{r^2}\frac{m(\xi)}{\overline{m'(\xi)}}, \qquad \mathrm{e}^{\mathrm{i}\alpha(z)} = \frac{\xi}{r}\frac{m'(\xi)}{|m'(\xi)|}, \qquad \mathrm{e}^{-\mathrm{i}\alpha(z)} = \frac{\overline{\xi}}{r}\frac{\overline{m'(\xi)}}{|m'(\xi)|}; \quad \xi = \mathrm{e}^{\mathrm{i}\theta} \text{ on } \Gamma, \tag{2.29}$$

Eq. (2.10) becomes

$$\begin{aligned} 2[[u_n + \mathrm{i}u_t]] &= \frac{\overline{\xi m'(\xi)}}{|\xi||m'(\xi)|}\left\{\frac{\kappa_1\phi_1(\xi) - \overline{\Omega_1(\xi)}}{\mu_1} - \frac{\kappa_2\phi_2(\xi) - \overline{\Omega_2(\xi)}}{\mu_2}\right\}, \quad \text{on } \Gamma, \\ 2[[u_n - \mathrm{i}u_t]] &= \frac{\xi m'(\xi)}{|\xi||m'(\xi)|}\left\{\frac{\kappa_1\overline{\phi_1(\xi)} - \Omega_1(\xi)}{\mu_1} - \frac{\kappa_2\overline{\phi_2(\xi)} - \Omega_2(\xi)}{\mu_2}\right\}, \quad \text{on } \Gamma. \end{aligned} \tag{2.30}$$

Similarly, Eq. (2.6) becomes

$$\sigma_{nn} - \mathrm{i}\sigma_{nt} = \frac{\phi'(\xi)}{m'(\xi)} + \overline{\frac{\phi'(\xi)}{m'(\xi)}} - \left\{ \left(\frac{\phi''(\xi)m'(\xi) - \phi'(\xi)m''(\xi)}{[m'(\xi)]^2} \right) \overline{\frac{m(\xi)}{m'(\xi)}} + \frac{\psi'(\xi)}{m'(\xi)} \right\} \mathrm{e}^{2\mathrm{i}\theta} \quad \text{on } \Gamma.$$

Multiplying the above expression by the (non-vanishing) factor $[m'(\xi)]^2\overline{m'(\xi)}$, and eliminating $\psi'(\xi)$ using Eq. (2.21), we obtain

$$[m']^2\overline{m'}[\sigma_{nn} - \mathrm{i}\sigma_{nt}] = (m')^2(\overline{\phi'} - \mathrm{e}^{2\mathrm{i}\theta}\Omega'). \tag{2.31}$$

Consequently, from Eqs. (2.11) and (2.29)–(2.31), the interface condition (2.9) becomes:

$$\begin{aligned}(m')^2(\overline{\phi'} - \mathrm{e}^{2\mathrm{i}\theta}\Omega') = {} & \left(\frac{h_1 - h_2}{4}\right)(m')^2\overline{m'}\frac{\overline{\xi m'}}{|\xi||m'|}\left[\frac{\kappa_1\phi_1 - \overline{\Omega}_1}{\mu_1} - \frac{\kappa_2\phi_2 - \overline{\Omega}_2}{\mu_2}\right] \\ & + \left(\frac{h_1 + h_2}{4}\right)(m')^2\overline{m'}\frac{\xi m'}{|\xi||m'|}\left[\frac{\kappa_1\overline{\phi}_1 - \Omega_1}{\mu_1} - \frac{\kappa_2\overline{\phi}_2 - \Omega_2}{\mu_2}\right] \\ & - \frac{(m')^2\overline{m'}}{|\xi||m'|}\left\{\frac{(h_1 - h_2)\overline{\xi m'}}{2}[\varepsilon_1 m + (\varepsilon_2 + \mathrm{i}\varepsilon_3)\overline{m}] + \frac{(h_1 + h_2)\xi m'}{2}[\varepsilon_1\overline{m} + (\varepsilon_2 - \mathrm{i}\varepsilon_3)m]\right\}.\end{aligned}$$

For thermal stresses resulting from a uniform change in temperature,

$$\varepsilon^0_{xx} = \varepsilon^0_{yy}, \qquad \varepsilon^0_{xy} = 0 \Rightarrow \varepsilon_1 = \varepsilon^0_{xx} = \varepsilon^0_{yy}, \qquad \varepsilon_2 = \varepsilon_3 = 0.$$

Using Eq. (2.12), we can eliminate ξ from the right-hand side of this expression and obtain:

$$\begin{aligned}(m')^2(\overline{\phi'} - \mathrm{e}^{2\mathrm{i}\theta}\Omega') = {} & \frac{bm'\sqrt{1 + b^*\sin^2\theta}}{4}\left\{(h_1 - h_2)\overline{m'}\mathrm{e}^{-\mathrm{i}\theta}\left[\frac{\kappa_1\phi_1 - \overline{\Omega}_1}{\mu_1} - \frac{\kappa_2\phi_2 - \overline{\Omega}_2}{\mu_2} - 2\varepsilon_1 m\right]\right\} \\ & + \frac{bm'\sqrt{1 + b^*\sin^2\theta}}{4}\left\{(h_1 + h_2)m'\mathrm{e}^{\mathrm{i}\theta}\left[\frac{\kappa_1\overline{\phi}_1 - \Omega_1}{\mu_1} - \frac{\kappa_2\overline{\phi}_2 - \Omega_2}{\mu_2} - 2\varepsilon_1\overline{m}\right]\right\},\end{aligned} \tag{2.32}$$

where $b^* = (a^2 - b^2)/b^2$. From Eqs. (2.23)–(2.28), noting that $\xi = \mathrm{e}^{\mathrm{i}\theta}$ on Γ, we obtain the final form of the interface condition (2.9):

$$(m')^2(\overline{\phi'} - \mathrm{e}^{2\mathrm{i}\theta}\Omega') = \frac{bRlm'\sqrt{1 + b^*\sin^2\theta}}{8}\left\{(h_1 - h_2)Q_n + (h_1 + h_2)\overline{Q}_n\right\} \quad z \in \Gamma, \tag{2.33}$$

where

$$Q_n = g_1 - g_2\mathrm{e}^{2\mathrm{i}\theta} - g_3\mathrm{e}^{-2\mathrm{i}\theta} + \sum_{n=0}^{\infty} M_n\xi^{-\mathrm{i}(n+2)\theta} - \sum_{n=0}^{\infty} N_n\xi^{\mathrm{i}n\theta} - \sum_{n=0}^{\infty} M_nR^{-2}\xi^{-\mathrm{i}n\theta} + \sum_{n=0}^{\infty} N_nR^{-2}\xi^{\mathrm{i}(n+2)\theta}, \tag{2.34}$$

$$\begin{aligned}& g_1 = -\varepsilon_1 lR + \frac{\varepsilon_1 l}{R^3}, \qquad g_2 = -\frac{\varepsilon_1 l}{R}, \qquad g_3 = \frac{\varepsilon_1 l}{R}, \qquad M_n = \Lambda_2\overline{D}_n + \Lambda_3 T_n, \\ & N_n = \Lambda_4\overline{E}_n + \Lambda_5 S_n, \qquad \Lambda_1 = \frac{1 + \kappa_1}{\mu_1}, \qquad \Lambda_2 = \frac{\kappa_1}{\mu_1} + \frac{1}{\mu_2}, \qquad \Lambda_3 = \frac{\kappa_1}{\mu_1} - \frac{\kappa_2}{\mu_2}, \\ & \Lambda_4 = \frac{1}{\mu_1} - \frac{1}{\mu_2}, \qquad \Lambda_5 = \frac{1}{\mu_1} + \frac{\kappa_2}{\mu_2}.\end{aligned} \tag{2.35}$$

Furthermore, in this case, we have

$$\varepsilon_1 = \frac{(\alpha_2 - \alpha_1)\Delta T}{2} = \frac{\Delta\alpha\Delta T}{2}, \tag{2.36}$$

where ΔT is the uniform change (cooling) in temperature and α denotes the coefficient of thermal expansion.

From Eqs. (2.12) and (2.23)–(2.28), the interface condition (2.33) becomes

$$\begin{aligned} &d_0 + d_1 e^{-i\theta} + d_2 e^{i\theta} + d_3 e^{-2i\theta} + d_4 e^{2i\theta} + d_5 e^{-3i\theta} + d_6 e^{-4i\theta} + \sum_{n=0}^{\infty} U_n e^{i(n+2)\theta} + \sum_{n=0}^{\infty} V_n e^{-i(n+4)\theta} \\ &\quad = \Lambda\left(\sqrt{1 + b^* \sin^2\theta}\right)\left[c_0 + c_1 e^{-i\theta} + c_2 e^{i\theta} + f_2 e^{2i\theta} + c_3 e^{-2i\theta} + c_4 e^{-3i\theta} + f_4 e^{-4i\theta}\right. \\ &\qquad \left. + \sum_{n=0}^{\infty} P_n e^{i(n+2)\theta} + \sum_{n=0}^{\infty} O_n e^{-i(n+4)\theta}\right], \end{aligned} \tag{2.37}$$

where

$$U_n = 2l^2[-R^4(\overline{T}_n + D_n)(n+1) + 2R^2(\overline{T}_{n+2} + D_{n+2})(n+3) - (\overline{T}_{n+4} + D_{n+4})(n+5)], \tag{2.38}$$

$$\begin{aligned} V_n = 2l^2[&-2R^2(T_{n+1} + \overline{D}_{n+1})(n+2) + 2(T_{n+3} + \overline{D}_{n+3})(n+4) + R^4(E_{n+4} + \overline{S}_{n+4})(n+5) \\ &- 2R^2(E_{n+2} + \overline{S}_{n+2})(n+3) + (E_n + \overline{S}_n)(n+1) + 2R^2(T_n + \overline{D}_n)(n+1) + (T_{n+2} + \overline{D}_{n+2})(n+3)], \end{aligned} \tag{2.39}$$

$$\begin{aligned} &P_n = L_{n+4} + G_{n+2} + J_n, \qquad O_n = F_{n+2} - H_{n+4} - K_n, \\ &F_n = 2(h_1 + h_2)R^{-2}\overline{N}_n + (h_1 - h_2)(1 + R^{-4})M_n, \\ &G_n = 2(h_1 + h_2)R^{-2}\overline{M}_n + (h_1 - h_2)(1 + R^{-4})N_n, \\ &H_n = (h_1 + h_2)\overline{N}_n + (h_1 - h_2)R^{-2}M_n, \\ &J_n = (h_1 + h_2)\overline{M}_n + (h_1 - h_2)R^{-2}N_n, \\ &K_n = [(h_1 + h_2)R^{-2}\overline{N}_n + (h_1 - h_2)M_n]R^{-2}, \\ &L_n = [(h_1 + h_2)R^{-2}\overline{M}_n + (h_1 - h_2)N_n]R^{-2}, \end{aligned} \tag{2.40}$$

$$\begin{aligned} &f_1 = (h_1 + h_2)(\overline{g}_1 - \overline{g}_3 R^{-2}) + (h_1 - h_2)(g_1 + g_2 R^{-2}), \\ &f_2 = (h_1 + h_2)\overline{g}_3 - (h_1 - h_2)g_2, \\ &f_3 = -(h_1 + h_2)(\overline{g}_2 + \overline{g}_1 R^{-2}) + (h_1 - h_2)(g_3 - g_1 R^{-2}), \\ &f_4 = [(h_1 + h_2)\overline{g}_2 - (h_1 - h_2)g_3]R^{-2}, \end{aligned} \tag{2.41}$$

$$\Lambda = \frac{b(a+b)^3}{2(a-b)}, \qquad c_0 = f_1 + L_2 + G_0 + H_0, \tag{2.42}$$

$$
\begin{aligned}
&c_1 = L_1 + H_1, \qquad c_2 = L_3 + G_1, \qquad c_3 = f_3 + L_0 + F_0 + H_2, \qquad c_4 = F_1 + H_3,\\
&d_0 = 4l^2R^2(\overline{T}_0 + D_0) - 6l^2(\overline{T}_2 + D_2) + 2l^2R^4(E_0 + \overline{S}_0),\\
&d_1 = -4l^2(\overline{T}_1 + D_1 - \overline{T}_0 - D_0) + 4l^2R^4(E_1 + \overline{S}_1),\\
&d_2 = 8l^2R^2(\overline{T}_1 + D_1) - 8l^2(\overline{T}_3 + D_3),\\
&d_3 = -2l^2(\overline{T}_0 + D_0 - 2T_0 - 2\overline{D}_0 - 4T_1 - 4\overline{D}_1) + 6l^2R^4(\overline{S}_2 + E_2) - 4l^2R^2(E_0 + \overline{S}_0),\\
&d_4 = 0,\\
&d_5 = -4l^2R^2(T_0 + \overline{D}_0 + 2E_1 + 2\overline{S}_1) + 4l^2(2T_1 + 2\overline{D}_1 + 3T_2 + 3\overline{D}_2) + 8l^2R^4(E_3 + \overline{S}_3),\\
&d_6 = 0.
\end{aligned}
\tag{2.43}
$$

In the above expressions, the coefficients T_i and E_i can be written in terms of S_i and D_i using Eq. (2.25). Hence, the only remaining unknown coefficients are again D_n and S_n.

Next, we employ a method similar to that used in Shen et al. (2000a,b) by substituting the following expression (valid for any positive number b^*, see Shen et al., 2000a,b) for $\sqrt{1 + b^* \sin^2\theta}$ into Eq. (2.37):

$$
\begin{aligned}
\sqrt{1 + b^* \sin^2\theta} &= \sum_{k=-\infty}^{\infty} I_{2k} e^{i2k\theta}\\
&\cong \sum_{k=0}^{\infty} I_{2k}(e^{i2k\theta} + e^{-i2k\theta}) + I_{2M}\frac{e^{i2M\theta} + e^{-i2M\theta} - \eta(e^{i2(M-1)\theta} + e^{i2(1-M\theta)})}{1 + \eta^2 - \eta(e^{i2\theta} + e^{-i2\theta})}\\
&= \sum_{k=0}^{\infty} I_{2k}(e^{i2k\theta} + e^{-i2k\theta}) + I_{2M}\frac{e^{i2M\theta} + e^{-i2M\theta} - \eta(e^{i2(M-1)\theta} + e^{i2(1-M\theta)})}{x - \eta(e^{i2\theta} + e^{-i2\theta})}.
\end{aligned}
\tag{2.44}
$$

We obtain

$$
\begin{aligned}
&\left[x_2 e^{-i\theta} + x_4 e^{-2i\theta} + x_6 e^{-3i\theta} + x_8 e^{-4i\theta} - x_{10} e^{-5i\theta} - x_{11} e^{-6i\theta} + x\sum_{n=0}^{\infty} V_n e^{-i(n+4)\theta} - \eta\sum_{n=0}^{\infty} V_n e^{-i(n+2)\theta}\right.\\
&\quad \left. - \eta\sum_{n=0}^{\infty} V_n e^{-i(n+6)\theta}\right] + x_1 + \left[x_3 e^{i\theta} + x_5 e^{2i\theta} - x_7 e^{3i\theta} - x_9 e^{4i\theta} + x\sum_{n=0}^{\infty} U_n e^{i(n+2)\theta}\right.\\
&\quad \left. - \eta\sum_{n=0}^{\infty} U_n e^{i(n+4)\theta} - \eta\sum_{n=0}^{\infty} U_n e^{in\theta}\right]\\
&\quad = \Lambda\left\{\left[\sum_{k=0}^{\infty} I_{2k}(e^{i2k\theta} + e^{-i2k\theta})(x - \eta(e^{i2\theta} + e^{-i2\theta})) + I_{2M}(e^{i2M\theta} + e^{-i2M\theta} - \eta(e^{i2(M-1)\theta}\right.\right.\\
&\qquad \left.\left. + e^{i2(1-M\theta)}))\right]\left[c_0 + c_1 e^{-i\theta} + c_2 e^{i\theta} + f_2 e^{2i\theta} + c_3 e^{-2i\theta} + c_4 e^{-3i\theta} + f_4 e^{-4i\theta} + \sum_{n=0}^{\infty} P_n e^{i(n+2)\theta}\right.\\
&\qquad \left. + \sum_{n=0}^{\infty} O_n e^{-i(n+4)\theta}\right]\right\},
\end{aligned}
\tag{2.45}
$$

where

$$\begin{aligned}
&\eta = \frac{1}{R^2}, \qquad x = 1 + \eta^2, \quad x_1 = xd_0 - \eta d_3, \quad x_2 = xd_1 - \eta d_5 - \eta d_2,\\
&x_3 = xd_2 - \eta d_1, \quad x_4 = xd_3 - \eta d_6 - \eta d_0, \quad x_5 = -\eta d_0, \quad x_6 = xd_5 - \eta d_1,\\
&x_7 = \eta d_2, \quad x_8 = xd_6 - \eta d_3, \quad x_9 = 0, \quad x_{10} = \eta d_5, \quad x_{11} = \eta d_6.
\end{aligned} \tag{2.46}$$

Furthermore, by equating coefficients of $e^{in\theta}$ in Eq. (2.45), we finally obtain

$$\sum_{k=0}^{M} W_{nk} I_{2k} = Q_n. \tag{2.47}$$

Hence W_{nk} and Q_n are finally related to coefficients S_i and D_i. For example, for $M = 5$ and $e^{i3\theta}(n = 3)$, we obtain

$$\begin{aligned}
&W_{30} = xP_1 - 2\eta P_3 - c_2\eta, \quad W_{31} = xP_3 - 2\eta P_1 - \eta P_5 + c_2 x - c_1\eta,\\
&W_{32} = xP_5 - \eta P_3 - \eta P_7 - c_4\eta + c_1 x - c_2\eta,\\
&W_{33} = xP_7 - \eta P_5 - \eta P_9 + c_4 x - c_1\eta - \eta O_1,\\
&W_{34} = xP_9 - \eta P_7 - \eta P_{11} - c_4\eta + xO_1 - \eta O_3,\\
&W_{35} = P_{11} - \eta P_9 - \eta O_1 + O_3; \qquad Q_3 = \frac{-x_7 + xU_1 - \eta U_3}{\Lambda}.
\end{aligned} \tag{2.48}$$

Depending on the level of accuracy required, we may select different values of M corresponding to a set of M linear equations and finally obtain the coefficients S_i and D_i.

3. Numerical example and discussion

Let $b = 1$ and consider the case of a silicon matrix surrounding a aluminum inclusion. The material properties are described by (Pottinger et al., 1994; Evans et al., 1991):

$$E_1 = 190 \text{ GPa}, \quad v_1 = 0.28, \quad \mu_1 = 74.22 \text{ GPa}, \quad \alpha_1 = 2.5 \times 10^{-6}/^{\circ}\text{C},$$

$$E_2 = 62 \text{ GPa}, \quad v_2 = 0.33, \quad \mu_2 = 23.31 \text{ GPa}, \quad \alpha_2 = 25 \times 10^{-6}/^{\circ}\text{C},$$

where E is Young's modulus and v is Poisson's ratio.

According to Hashin (1991b), the imperfect interface condition arises from the assumption of a thin compliant layer of thickness $t \ll b$ with shear modulus $\mu_c \ll \min\{\mu_1, \mu_2\}$ between the inclusion and the matrix. This defines the physical meaning of the parameter h. Therefore, the imperfect interface parameter h may be determined by the properties and thickness of the thin compliant layer.

In practice, the imperfect interface parameter h is rendered dimensionless by division by μ_1/b, where μ_1 is the shear modulus of the matrix, and b is the minor axis of the ellipse. In this calculation, two cases are considered, $h_1 = h_2$ and $h_1 = 3h_2$ (basically, the imperfect interface parameters are related to Young's modulus and Shear's modulus, Hashin, 1991b). The results from these two cases are compared and discussed.

In what follows, we present results for three different ranges of the aspect ratio a/b. In each case, the number of coefficients in the corresponding series is chosen so that the error in the numerical calculations is maintained below 1%. This is achieved simply by calculating an increasing sequence of partial sums from each of the (uniformly convergent) infinite series representations and noting the minimum number of coefficients required to ensure that the difference between any two subsequent partial sums is less than 1% (see Shen et al., 2000a).

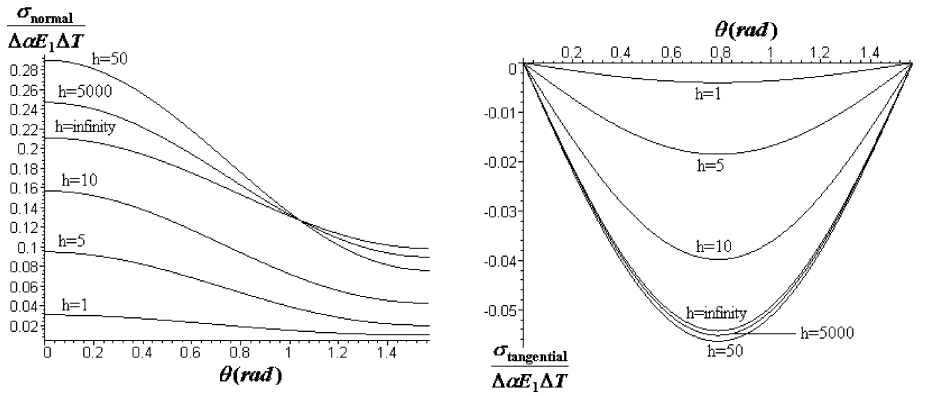

Fig. 2. Normal and tangential stresses along the interface for $a/b = 3.5$ in plane strain under a uniform change in temperature for $h_1 = h_2 = h$.

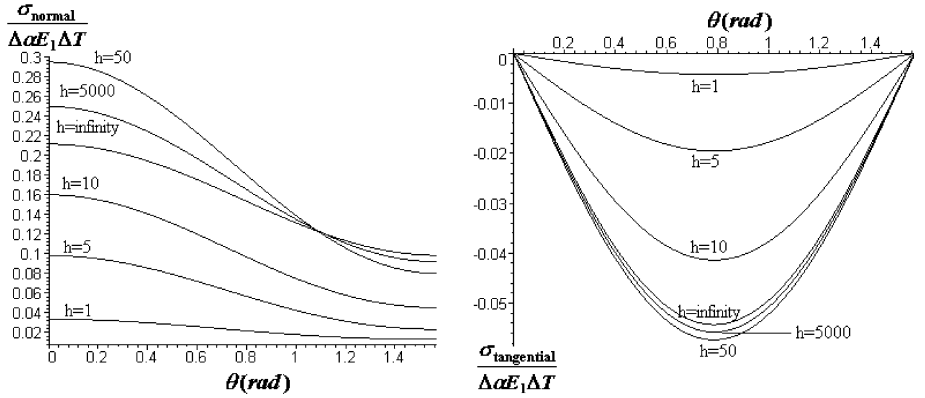

Fig. 3. Normal and tangential stresses along the interface for $a/b = 3.5$ in plane strain under a uniform change in temperature for $h_1 = 3h_2 = h$.

Case 1. When $1 < a/b \leqslant 3.5$, only the coefficients $S_0(D_0)$, $S_1(D_1)$ and $S_2(D_2)$ are necessary to achieve the desired accuracy. From Eqs. (2.24) and (2.25), considering Eq. (2.12), it is easy to find ϕ_2 and Ω_2 expressed in terms of $S_0(D_0)$, $S_1(D_1)$ and $S_2(D_2)$. Furthermore, ψ_2 can be obtained from Eq. (2.21). For example, in the present case

$$\phi_2(z) \cong -\frac{2S_1}{R^2} + \left(\frac{S_0}{R} - \frac{3S_2}{R^3}\right)\left(\frac{2z}{l}\right) + \frac{S_1}{R^2}\left(\frac{2z}{l}\right)^2 + \frac{S_2}{R^3}\left(\frac{2z}{l}\right)^3. \tag{3.1}$$

Once ϕ_2 and ψ_2 are obtained, we can calculate the stress distribution inside the inclusion. In Figs. 2 and 3, the stress distribution along the interface (normal and tangential directions) in the two cases $h_1 = h_2$ and $h_1 = 3h_2$ is plotted for the value $a/b = 3.5$ and different values of the parameter h. When $h = 50$, the local stresses reach maximum values for both cases. For the present problem, it is found that there is no significant difference between the cases $h_1 = h_2$ and $h_1 = 3h_2$. This is due to the fact that the interfacial stresses caused by thermal contraction of the inclusion are dominated by the normal component so that the role of the tangential interface parameter h_2 is insignificant. Hence, for practical inclusion (structural) design, to satisfy the basic requirements we need only consider the case $h_1 = h_2$ or $h_1 = 3h_2$.

Case 2. When $3.5 < a/b \leqslant 7$, only the coefficients $S_0(D_0)$, $S_1(D_1)$, $S_2(D_2)$ and $S_3(D_3)$ are necessary to achieve the desired accuracy. As above, we can obtain ϕ_2, Ω_2 and ψ_2 expressed in terms of $S_0(D_0)$, $S_1(D_1)$, $S_2(D_2)$ and $S_3(D_3)$. The corresponding interfacial stress distributions are presented in Figs. 4 and 5.

Case 3. When $7 < a/b \leqslant 10$, only the coefficients $S_0(D_0)$, $S_1(D_1)$, $S_2(D_2)$, $S_3(D_3)$ and $S_4(D_4)$ are necessary to achieve the desired accuracy. Again, we can obtain ϕ_2, Ω_2 and ψ_2 expressed in terms of $S_0(D_0)$, $S_1(D_1)$, $S_2(D_2)$, $S_3(D_3)$ and $S_4(D_4)$. The corresponding interfacial stress distributions are presented in Figs. 6 and 7.

It is noted that for values $a/b > 10$ of the aspect ratio, the procedure is similar although a much larger number of coefficients is required to evaluate the corresponding series to the desired accuracy.

From Figs. 2–7, it is clear that the homogeneously imperfect interface parameter h significantly influences the stress distribution although the aspect ratio of the elliptic inclusion does not significantly change the locations of the maximum normal and tangential tractions along the interface and their magnitudes. It is found that the normal stresses are always positive along the entire interface. Consequently, any possible overlapping associated with the imperfect interface model used in this paper (see, Achenbach and Zhu, 1990; Hashin, 1991b) cannot occur in the present thermal stress problem.

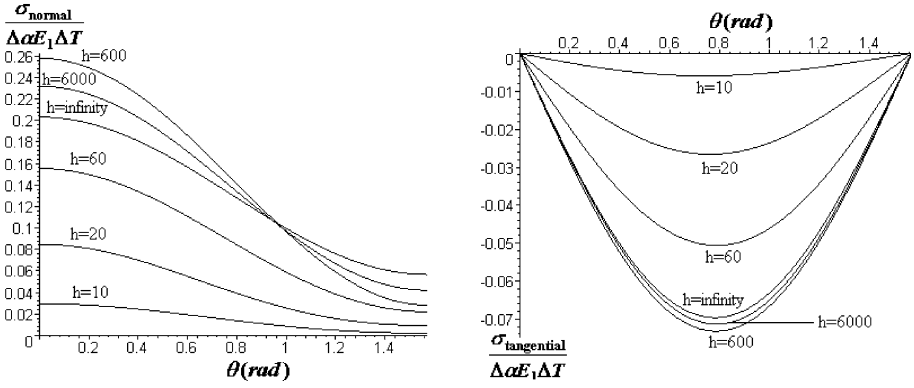

Fig. 4. Normal and tangential stresses along the interface for $a/b = 7$ in plane strain under a uniform change in temperature for $h_1 = h_2 = h$.

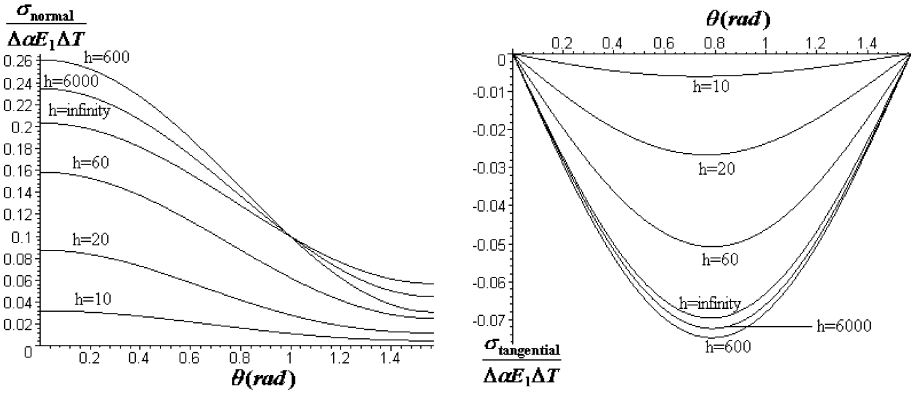

Fig. 5. Normal and tangential stresses along the interface for $a/b = 7$ in plane strain under a uniform change in temperature for $h_1 = 3h_2 = h$.

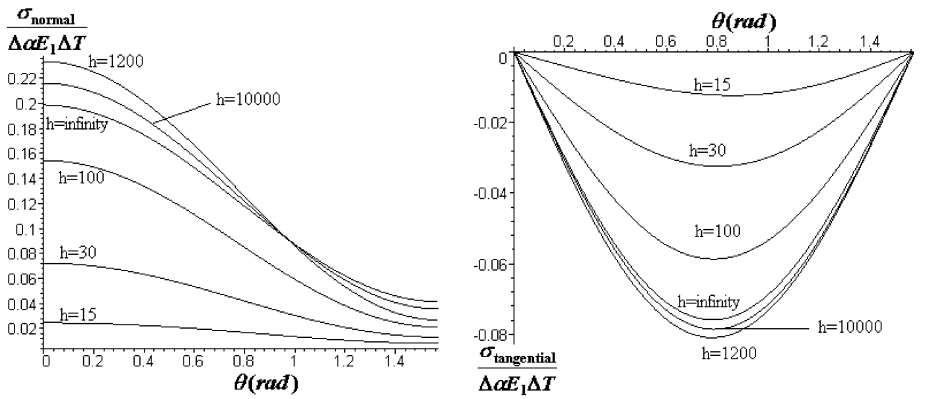

Fig. 6. Normal and tangential stresses along the interface for $a/b = 10$ in plane strain under a uniform change in temperature for $h_1 = h_2 = h$.

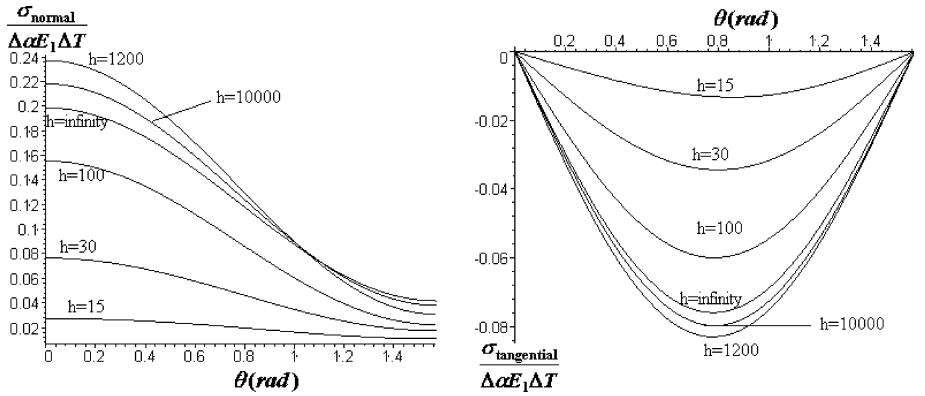

Fig. 7. Normal and tangential stresses along the interface for $a/b = 10$ in plane strain under a uniform change in temperature for $h_1 = 3h_2 = h$.

Again, since Figs. 2–7 show no significant difference in the results obtained between the cases $h_1 = h_2$ and $h_1 = 3h_2$, the following discussions are based solely on the results from the case $h_1 = 3h_2 = h$.

We employ two different methods to analyze and understand the relationship between the imperfect interface parameter h and the failure of the interface. Firstly, we calculate the peak resultant traction (stress) along the interface (henceforth referred to as the peak traction).

The peak traction is found by calculating the maximum value of the resultant traction $\sigma_{\text{resultant}}/(\Delta\alpha E_1 \Delta T)$ (Hu, 1991) along the interface for a given aspect ratio and a given value of the parameter h. Here, $\sigma_{\text{resultant}}$ is defined by the relation

$$\sigma_{\text{resultant}} = \sqrt{\sigma^2_{\text{normal}} + \sigma^2_{\text{tangential}}} \tag{3.2}$$

and $\Delta\alpha E_1 \Delta T$ represents the stress induced by the uniform change (cooling) in the matrix temperature. This peak traction is found always to occur at the point $\theta = 0$. Fig. 8 plots the peak traction as a function of the imperfect interface parameter h for different aspect ratios.

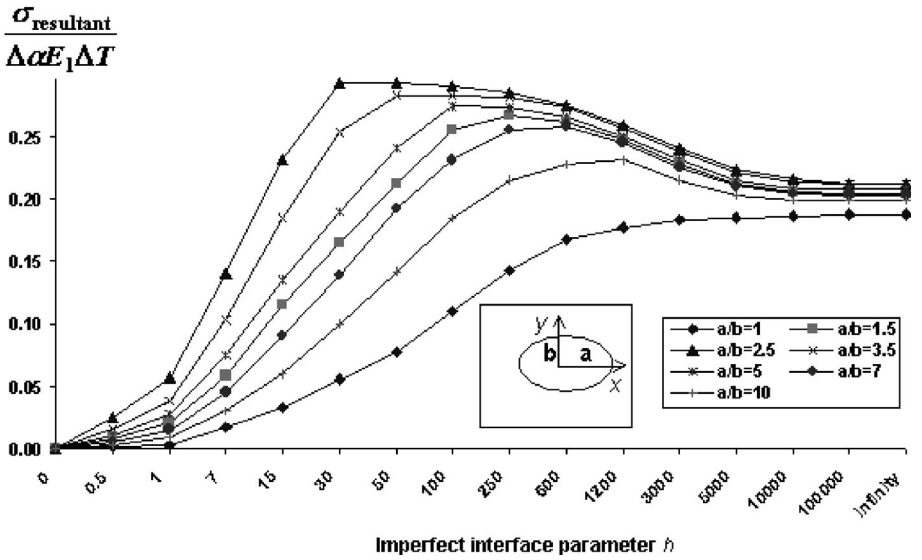

Fig. 8. The peak resultant traction along the interface varies as a function of the imperfect interface parameter h in plane strain under a uniform change in temperature for $h_1 = 3h_2 = h$.

From Fig. 8, it is clear that, for each aspect ratio (except $a/b = 1$ which is discussed below), the peak traction is a non-monotonic function of the interface parameter h. Consequently, for each aspect ratio, there is a unique value of the interface parameter h which corresponds to maximum peak traction. The collection of these values of h define the parameter h^* (see Fig. 13).

In contrast to the results established for the circular inclusion where the maximum peak traction appears at $h = \infty$ (Ru, 1998b), the results established here indicate that the maximum peak traction for an elliptic inclusion depends on the imperfect interface parameter and the aspect ratio of the ellipse. To explain this, we note that for the present interphase layer model (Hashin, 1991b), in order to keep the thickness of the adhesive layer between the elliptic inclusion and the matrix uniform (the "equal thickness" assumption mentioned in Section 1), unlike the innermost edge, the outer edge of the interphase layer cannot be elliptical. This is perhaps why, in the case of a homogeneously imperfect interface, values of h^* correspond to different values of local maximum peak stress for different values of the aspect ratio a/b (for the circular inclusion with homogeneously imperfect interface the outer edge of the interphase layer is circular). This makes the stress distributions within the elliptic inclusion intrinsically non-uniform.

Next we consider the strain energy density criterion used by Achenbach and Zhu (1990). For the simple interphase model considered here, the strain energy criterion is particularly appropriate since it includes the effects of both normal and shear tractions across the interphase. The energy per unit interphase, U, is defined as:

$$U = \frac{\sigma_{\text{normal}}^2}{2h_1} + \frac{\sigma_{\text{tangential}}^2}{2h_2}.$$

By introducing $\overline{\sigma}_{\text{normal}} = \sigma_{\text{normal}}/(\Delta\alpha E_1 \Delta T)$ and $\overline{\sigma}_{\text{tangential}} = \sigma_{\text{tangential}}/(\Delta\alpha E_1 \Delta T)$, we obtain, in dimensionless form:

$$\overline{U} = \frac{\overline{\sigma}_{\text{normal}}^2}{2h_1} + \frac{\overline{\sigma}_{\text{tangential}}^2}{2h_2}. \tag{3.3}$$

It is now reasonable to assume that the interface will fail when $\overline{U}$ reaches a critical value, $\overline{U}_{cr}$, which depends on the material properties. Figs. 9–11 plot the interfacial strain energy distribution along the interface for different aspect ratios of the ellipse in the case $h_1 = 3h_2 = h$. It is shown that the compliant layer (described by the homogeneously imperfect interface parameter h) does significantly influence the interfacial strain energy distribution. In particular, when h reaches a specific value, the peak interfacial strain energy reaches its maximum value.

Fig. 12 plots the peak (defined as in the case of peak traction above) strain energy per unit interphase $\overline{U}$ as a function of the imperfect interface parameter h $(= h_1 = 3h_2)$. It is clear from Fig. 12 that $\overline{U}$ is again a non-monotonic function of the interface parameter h. This means that we can again define a new parameter h^* defined by values of h which correspond to maximum values of the peak strain energy per unit interphase along the inclusion–matrix interface (see Fig. 14).

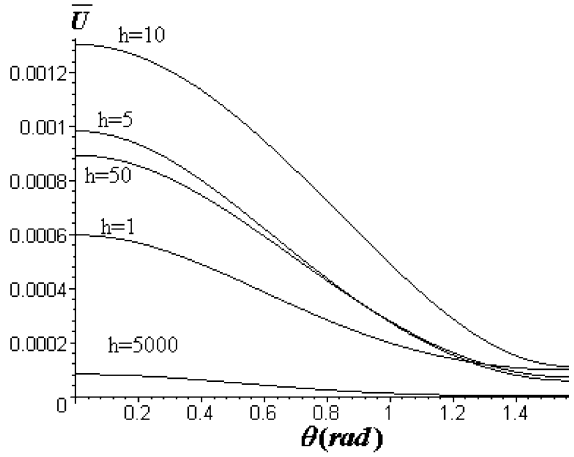

Fig. 9. The interfacial strain energy ($\overline{U}$) along the interface for $a/b = 3.5$ in plane strain under a uniform change in temperature for $h_1 = 3h_2 = h$.

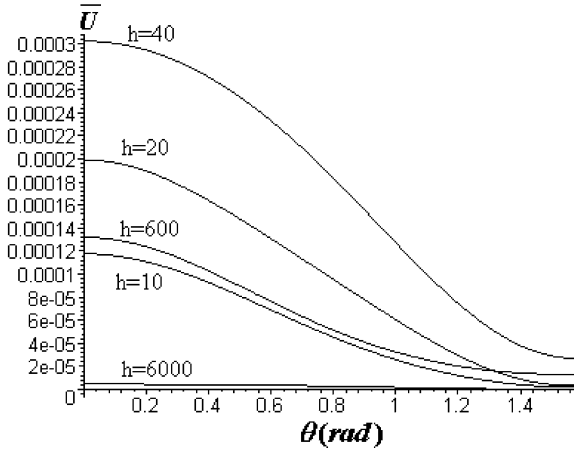

Fig. 10. The interfacial strain energy ($\overline{U}$) along the interface for $a/b = 7$ in plane strain under a uniform change in temperature for $h_1 = 3h_2 = h$.

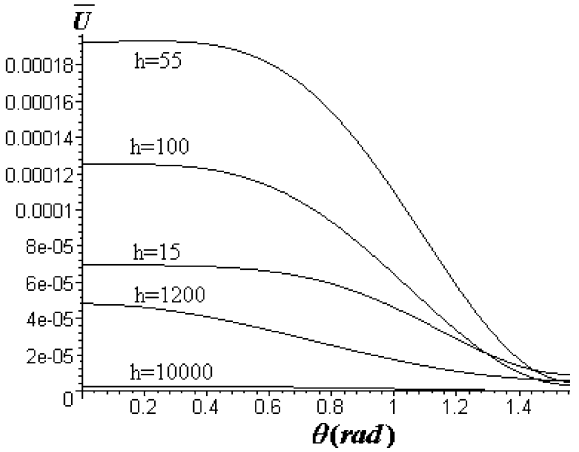

Fig. 11. The interfacial strain energy ($\overline{U}$) along the interface for $a/b = 10$ in plane strain under a uniform change in temperature for $h_1 = 3h_2 = h$.

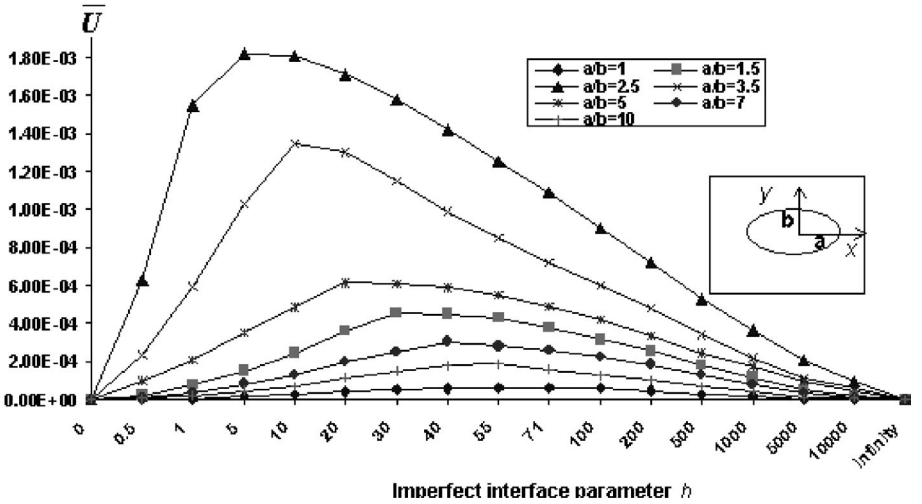

Fig. 12. The peak interfacial strain energy density varies as a function of the imperfect interface parameter h in plane strain under a uniform change in temperature for $h_1 = 3h_2 = h$.

We pause briefly to consider the case of the aspect ratio $a/b = 1$ (circular inclusion). For $a/b = 1$, from Fig. 8, the peak traction is no longer a non-monotonic function of the interface parameter h with the value of h^* occurring at $h^* = \infty$ (as in Ru, 1998b). From Fig. 12, however, $\overline{U}$ is indeed a non-monotonic function of the interface parameter h with $h^* \sim 71$. In addition, from Fig. 12, we may conclude that, since h^* appears only within a range corresponding to minimal stiffness of the spring layer, the energy density criterion is suitable for extremely soft (compliant) interphase layers. According to Hashin (1991b), the imperfect interface condition arises from the assumption of a thin flexible coating of thickness $t \ll b$ with shear modulus $\mu_c \ll \min\{\mu_1, \mu_2\}$ between the inclusion and the matrix. The physical meaning of the parameter h and the energy density criterion are therefore consistent with Hashin's definition.

It should be mentioned here that Achenbach and Zhu (1990) define the strain energy density by the strain energy of the interphase layer per unit length along the interface. If the critical value of the strain energy density corresponding to interfacial failure is of interest, a physically more reasonable definition is $\overline{U}_{cr}$ (as defined above) divided by the thickness of the interphase layer since this more appropriately represents the strain-energy density of the interphase material. In adopting this new definition, it is readily seen that the critical value $\overline{U}_{cr}$ should be proportional to the thickness of the interphase layer and that it then approaches zero as the thickness of the interface layer vanishes (which corresponds to $h = \infty$, since h is inversely proportional to the thickness of the interphase layer).

Since values of h^* correspond to local maximum peak stresses and maximum peak values of $\overline{U}$ and are related to the mechanical properties and thickness of the adhesive layer between the inclusion and the matrix, the parameter h^* may be used as a control parameter when designing "thermal inclusions" (Hu, 1991). For example, in the case of a uniform change (cooling) in temperature and the aspect ratio $a/b = 1$ (circular inclusion), the peak traction in Fig. 8 corresponds to the value $h^* = \infty$ (perfect bonding). However, when $a/b = 3.5$, the peak traction corresponds to $h^* = 50$. Since h^* is rendered dimensionless by division by μ_1/b, for a specific aspect ratio, we can avoid the maximum peak traction, or indeed minimize the maximum peak traction by adjusting μ_1 (the shear moduli of the matrix), and the thickness of the interphase layer (related to b).

In addition, from Figs. 8 and 12, we note that the effect of the interphase layer (the interface parameter h) on the peak traction and peak strain energy density is sensitive to small aspect ratios ($\leqslant 5$) of the elliptic inclusion, but not to larger values of a/b. It should be emphasized that in the present case, the normal stresses are always dominant compared to the shear stresses (see Figs. 2–8). This explains why other parameters such as the interfacial strain energy are not significantly affected when we use different values of h_2 (which is related to the shear stress).

The relationship between the parameter h^* and the aspect ratio a/b is presented in Figs. 13 and 14 for the two different failure criteria.

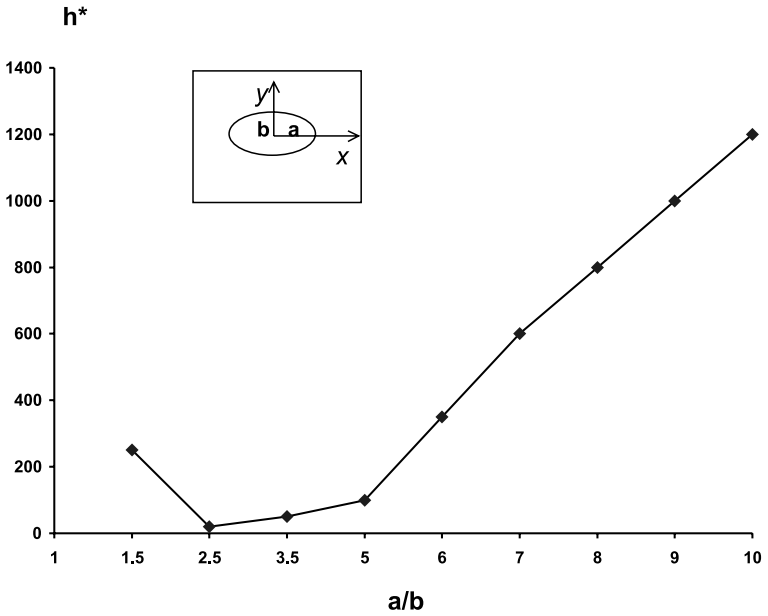

Fig. 13. The relationship between h^* and a/b using the resultant traction criterion when $h_1 = 3h_2 = h$.

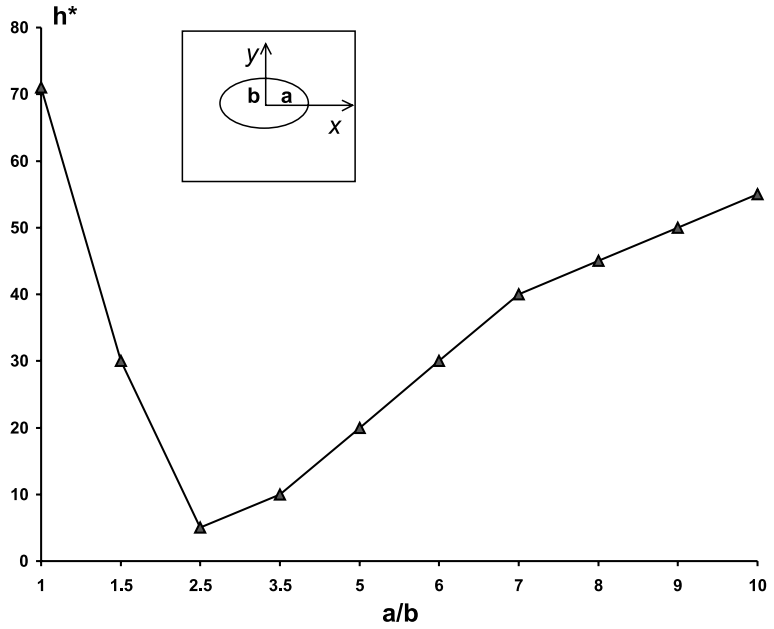

Fig. 14. The relationship between h^* and a/b using the interfacial strain energy density criterion for $h_1 = 3h_2 = h$.

4. Conclusions

The effect of a compliant interphase layer on residual stresses induced by a thermal mismatch is analyzed for the plane deformations of an elliptic inclusion in which the interphase layer is modeled as an imperfect interface. Particular emphasis is placed on the interfacial thermal stress distribution. Numerical computations and analysis of the subsequent results have led to the following conclusions:

1. The compliant interphase layer has a significant effect on the stress distribution along the interface. In particular, it has been shown that the effect of the interphase layer (described by the interface parameter h) on the peak traction and peak interfacial strain energy density is particularly significant for an elliptic inclusion with relatively small aspect ratio ($\leqslant 5$), but not for larger values of a/b.

2. The peak interfacial traction and peak interfacial strain energy density have been found to be non-monotonic functions of the interface parameter (h) describing the compliant interphase layer. Consequently, for different aspect ratios, we have identified a unique finite value h^* of the parameter h ($\neq 0, \infty$) which corresponds to maximum peak traction or maximum peak interfacial strain energy density along the interface. Hence, since the parameter h is determined by the properties and thickness of the adhesive layer between the elliptic inclusion and the matrix, it is possible to control the debonding and failure of the interface by designing the value h for a given aspect ratio. This means that, for a specific aspect ratio, it is possible to minimize peak interfacial stress by adjusting the mechanical properties or thickness of the adhesive layer.

3. It has been indicated that the normal stresses are always positive along the entire interface. Therefore, any possible overlapping associated with the imperfect interface model used in this paper cannot occur in the present problem. This result shows that the imperfect interface model is particularly suitable for thermal stress analysis of elastic inclusions with a compliant interphase layer.

4. The present computations also indicate that there is no significant difference between the cases $h_1 = h_2$ and $h_1 = 3h_2$. This is due to the fact that the interfacial stresses caused by thermal contraction of the inclusion are dominated by the normal component so that the tangential interface parameter h_2 plays an insignificant role.

Acknowledgements

This work was supported by the Natural Sciences and Engineering Research Council of Canada through grant NSERC OGP 115112.

References

Achenbach, J.D., Zhu, H., 1989. Effect of interfacial zone on mechanical behavior and failure of hexagonal-array fibre composites. J. Mech. Phys. Solids. 37, 381–393.

Achenbach, J.D., Zhu, H., 1990. Effect of interphase on micro and macromechanical behavior and failure of fibre-reinforced composites. J. Appl. Mech. 57, 956–963.

Dao, M., Gu, P., Maewal, A., Asaro, R.J., 1997. A micromechanical study of residual stresses in functionally graded materials. Acta Mater. 45, 3265–3276.

England, A.H., 1971. Complex variable methods in elasticity. London, Wiley-Interscience.

Evans, J.Y., Evans, J.W., 1991. Electronic materials and properties. In: Pecht, M. (Ed.), Handbook of Electronic Package Design. Marcel Dekker, New York.

Gao, J., 1995. A circular inclusion with imperfect interface: Eshelby's tensor and related problems. J. Appl. Mech. 62, 860–866.

Gleixner, R.J., Clements, B.M., Nix, W.D., 1997. Void nucleation in passivated interconnect lines: effect of site geometries, interfaces, and interface flaws. J. Mater. Res. 12 (8), 2081–2090.

Gong, S.X., Meguid, S.A., 1993. On the elastic fields of an elliptical inhomogeneity under plane deformation. Proc. R. Soc. Lond. A 443, 457–471.

Gouldstone, A., Shen, Y.-L., Suresh, S., Thompson, C.V., 1998. Evolution of stress in passivated and unpassivated metal interconnects. J. Mater. Res. 13 (7), 1956–1966.

Hashin, Z., 1990. Thermoelastic properties of fiber composites with imperfect interface. Mech. Mater. 8, 333–348.

Hashin, Z., 1991a. Thermoelastic properties of particulate composites with imperfect interface. J. Mech. Phys. Solids 39, 745–762.

Hashin, Z., 1991b. The spherical inclusion with imperfect interface. J. Appl. Mech. 58, 444–449.

Hu, S.M., 1991. Stress-related problems in silicon technology. J. Appl. Phys. 70, R53–R80.

Jasiuk, I., Tong, Y., 1989. The effect of interface on the elastic stiffness of composites. In: Reddy, J.N. (Ed.), Mechanics of Composite Materials and Structures, ASME AMD vol. 100, p. 49–54.

Korhonen, M.A., Paszkiet, C.A., Li, C.Y., 1991. Mechanisms of thermal stress relaxation and stress-induced voiding in narrow aluminum-based metallizations. J. Appl. Phys. 69, 8083–8091.

Lee, Y.D., Erdogan, F., 1995. Residual/thermal stresses in FGM and laminated thermal barrier coatings. Int. J. Fract. 69, 145–165.

Muskhelishvili, N.I., 1963. Some basic problems of the mathematical theory of elasticity. Groningen, Noodhoff.

Niwa, H., Yagi, H., Tsuchikawa, H., 1990. Stress distribution in an aluminum interconnect of very large scale integration. J. Appl. Phys. 68, 328–333.

Pottinger, M., Coburn, J., Edman, I., 1994. Journal of Polymer Science – part B: Polymer Physics 32 (5), 15–23.

Qu, J., 1993. Eshelby tensor for an elastic inclusion with slightly weakened interface. J. Appl. Mech. 60, 1048–1050.

Ru, C.Q., 1998a. Effect of interphase layers on thermal stresses within an elliptical inclusion. J. Appl. Phys. 84, 4872–4879.

Ru, C.Q., 1998b. A circular inclusion with circumferentially inhomogeneous sliding interface in plane elastostatics. J. Appl. Mech. 65, 30–38.

Ru, C.Q., Schiavone, P., 1997. A circular inclusion with circumferentially inhomogeneous interface in antiplane shear. Proc. R. Soc. London A 453, 2551–2572.

Ru, C.Q., Schiavone, P., Mioduchowski, A., 1999. Uniformity of stresses within a three-phase elliptic inclusion in anti-plane shear. J. Elasticity 52, 121–128.

Shen, H., Schiavone, P., Ru, C.Q., Mioduchowski, A., 2000a. An elliptic inclusion with imperfect interface in anti-plane shear. Int. J. Solids Struct. 37, 4557–4575.

Shen, H., Schiavone, P., Ru, C.Q., Mioduchowski, A., 2000b. Analysis of internal stress in an elliptic inclusion with imperfect interface in plane elasticity. Math. Mech. Solid 5, 501–521.

Shen, Y.-L., 1998. Stresses, deformation, and void nucleation in locally debonded metal interconnects. J. Appl. Phys. 84, 5525–5530.

Stagni, L., 1991. Elastic field perturbation by an elliptic inhomogeneity with a sliding interface. J. Appl. Math. Phys. (ZAMP) 42, 811–819.

Tsuchida, E., Mura, T., Dundurs, J., 1986. The elastic field of an elliptic inclusion with a slipping interface. J. Appl. Mech. 53, 103–107.

Wikström, A., Gudmundson, P., Suresh, S., 1999. Thermoelastic analysis of periodic thin lines deposited on a substrate. J. Mech. Phys. Solids. 47, 1113–1130.

Williamson, R.L., Rabin, B.H., Drake, J.T., 1993. Finite element analysis of thermal residual stresses at graded ceramic–metal interfaces model – part I: description and geometrical effects. J. Appl. Phys. 74, 1310–1320.

Wu, C.C., Kahn, M., Moy, W., 1996. Piezoelectric ceramics with functional gradients: a new application in material design. J. Am. Ceram. Soc. 79, 809–812.

Yeo, I.-S., Anderson, S.G., Ho, P.S., Hu, C.K., 1995. Characteristics of thermal stresses in Al(Cu) fine lines. II. Passivated line structures. J. Appl. Phys. 78, 953–961.